BNL-229823-2026-TECH

HSR Lattice Model in the Hadron Beam Direction Featuring High-Order Dipole Field Harmonics

G. Robert-Demolaize

May 2026

Electron-Ion Collider

Brookhaven National Laboratory

U.S. Department of Energy

USDOE Office of Science (SC), Nuclear Physics (NP)

DISCLAIMER

HSR Lattice Model in the Hadron Beam Direction Featuring High-Order Dipole Field Harmonics

G. Robert-Demolaize, J. S. Berg[1]

[1] *Brookhaven National Laboratory*

(Dated: May 28, 2026)

This note presents a contemporaneous lattice design for the EIC HSR ring using the 250730a release for 275GeV protons as a reference. The lattice is modified to replace the hadron cooling section in IR2 with a RHIC-like layout similar to the other non-colliding HSR insertions, and to follow the hadron beam direction i.e. counterclockwise. Another upgrade is the inclusion of the high-order field harmonics of the bending dipoles as derived from RHIC's `magbase` database. For the purposes of this document, only the sextupole harmonics ($b2$) are discussed. The impact of these harmonics on the baseline betatron tunes $Q_{x,y}$ and chromaticities $\chi_{x,y}$ is discussed, as well as the calculation and correction of the first two non-linear chromaticity terms $\chi_{x,y}^{(2,3)}$.

CONTENTS

I. UPDATING THE REFERENCE HSR DESIGN

The Electron Ion Collider (EIC) Hadron Storage Ring (HSR) [1, 2] is built from the exisitng Relativistic Heavy Ion Collider (RHIC) Yellow ring and features one interaction region (IR6). Its most recent lattice design to be used in accelerator codes (MAD-X [3], Xsuite [4], Bmad [5]) preserves the layout of insertion regions IR8 (formally host to the sPHENIX detector), IR10, IR12 and IR4. The IR6 insertion, previously occupied by the STAR detector, is going through a major layout overhaul to remain an interaction region: hadron bunches circulating in the HSR will collide with electron bunches from the Electron Storage Ring (ESR) [6] inside the ePIC detector [7].

Another major feature of the HSR lattice design is the repurposing of the IR2 insertion in order to accomodate the layout requirements for strong hadron cooling [8, 9]. However, recent studies [10] have led to high-energy cooling of hadron bunches to be deferred to a later upgrade. The official HSR lattice release `250730a` features the upgraded IR6 and IR2 insertion layouts, but one can quite easily revert IR2 to its RHIC-like configuration. Figure 1 shows a sample survey plot of the `250730a` HSR lattice after that revert. Figure 2 presents the linear optics functions $\beta_{x,y}$ and the dispersion D_x as a function of the longitudinal position S along the reference orbit in the beam direction.

For the purpose of depicting the counterclockwise (CCW) motion of hadron bunches circulating in the HSR, the ordering of the sequence of elements is reflected, and the reference frame of the design trajectory is modified: S is still counted positive going forward, Y is still counted positive going up, however X is now counted positive going towards the inside of the ring. To account for that change, the sign of all even-order magnetic elements and field harmonics (i.e. dipoles, sextupoles, and so forth) must be flipped from the initial `250730a` design. The sign of the dispersion function shown in Figure 2 is therefore flipped compared to what one would traditionally expect. Table I lists the baseline lattice parameters that are used as a reference for the rest of the studies in this document.

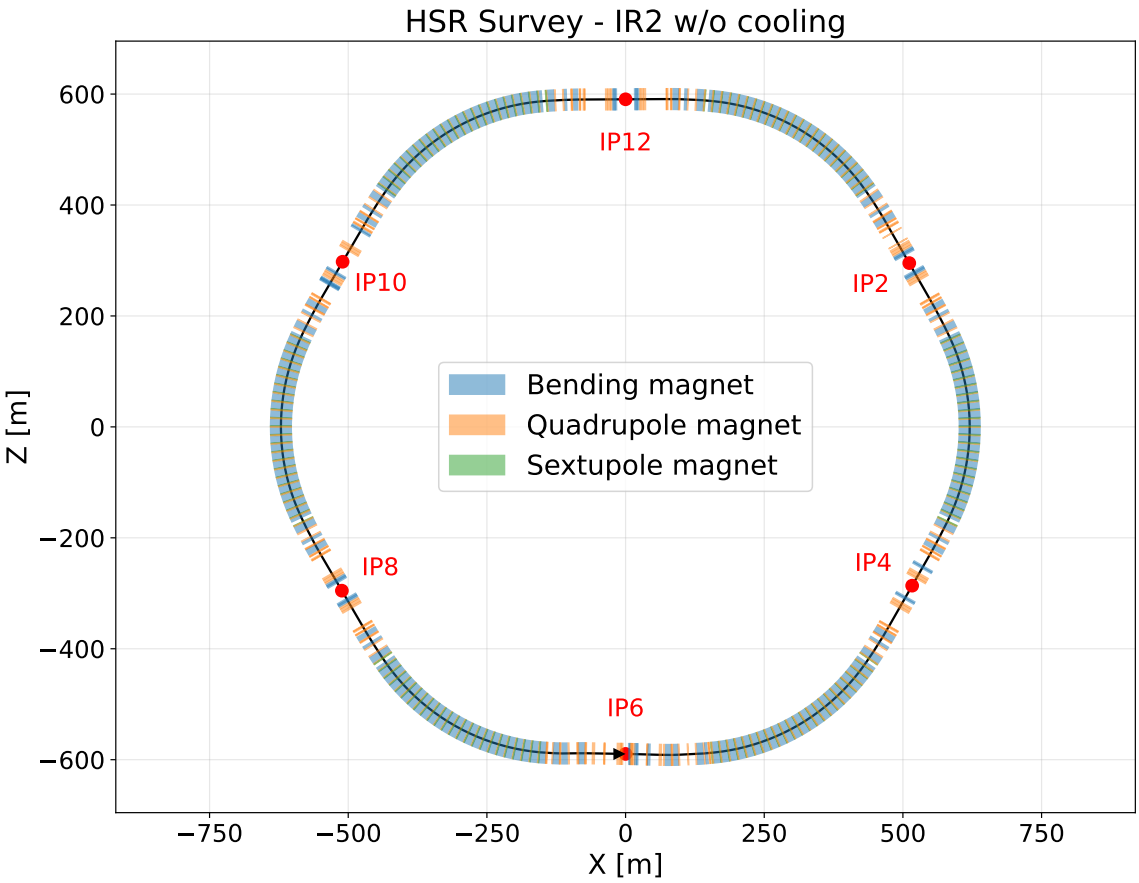

FIG. 1: Sample survey of the `250730a` HSR lattice with the upgraded IR6 for the ePIC detector and a RHIC-like layout in IR2 instead of the long drift section for strong hadron cooling. The hadron beam direction is counterclockwise. The location of the center of each insertion region (IP2-through-12) is given as a reference.

TABLE I: Main parameters of the HSR `250730a` lattice release for 275 GeV polarized protons.

Parameter	Symbol	Unit	Value
Beam species	—		proton
Beam energy	E	GeV	275
Reference energy	p_0c	GeV	274.998
Magnetic rigidity	$B\rho$	T m	917.296
Circumference	C	m	3833.845
Transition gamma	γ_t		22.58
Momentum compaction	α_c		1.96×10^{-3}
Working point	Q_x, Q_y	2π	28.228, 27.210
Chromaticities	χ_x, χ_y		2.00, 2.00
Cell phase advance	μ_x, μ_y	degrees	79.6, 80.2
Cell length	L_{cell}	m	29.66 m
Interaction-point beta functions	β_x^*, β_y^*	m	(0.800, 0.072)
Interaction-point dispersion	D_x^*, D_y^*	m	0, 0
Periodic arc beta functions	β_x, β_y	m	43.322, 12.458
Periodic arc dispersion (peak)	D_x	m	1.74
Maximum beta functions	$\beta_{x,\max}, \beta_{y,\max}$	m	1300, 1181
Maximum dispersion	$D_{x,\max}$	m	1.86

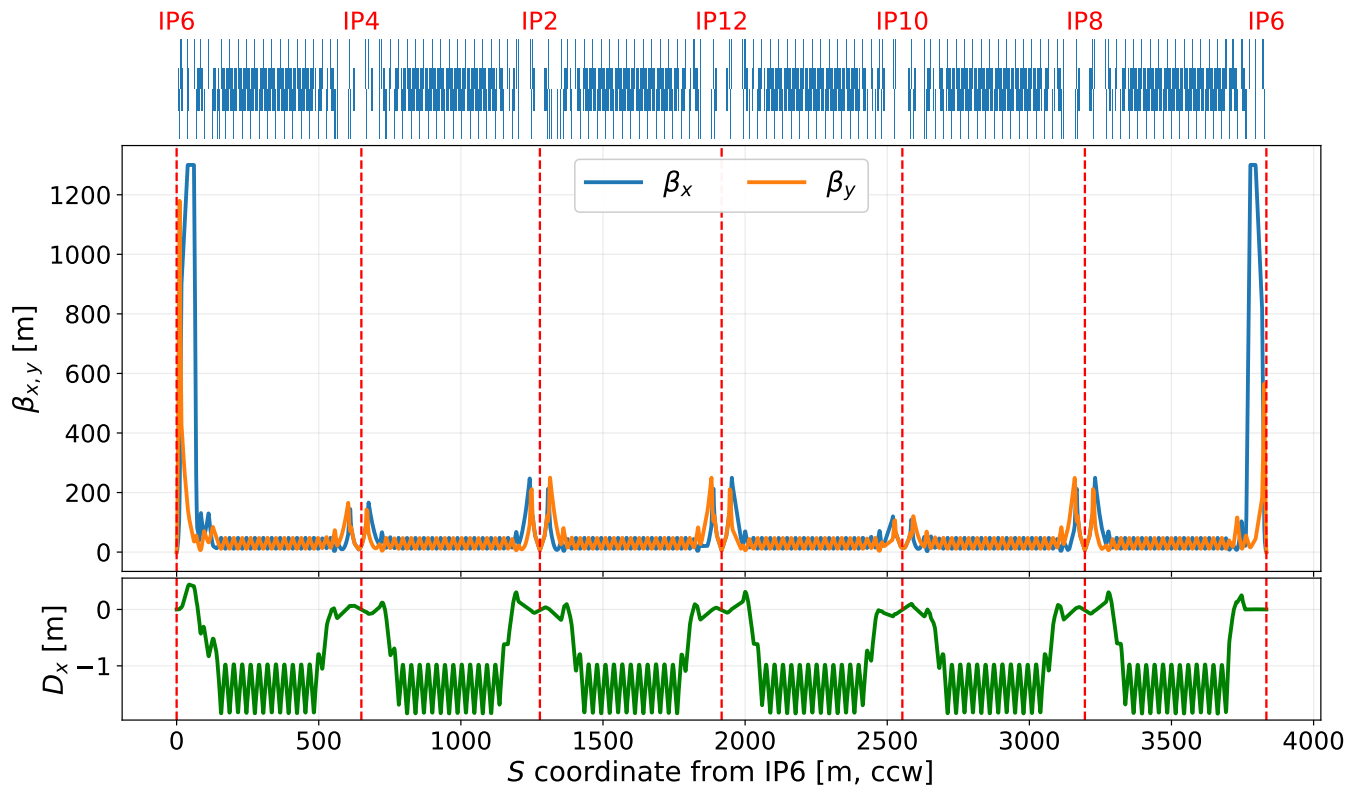

FIG. 2: Linear optics functions $\beta_{x,y}$ and dispersion D_x of the `250730a` HSR lattice with the upgraded IR6 for the ePIC detector and a RHIC-like layout in IR2. The hadron beam direction is counterclockwise, shown here left-to-right. The location of the center of each insertion region (IP2-through-12) is given as a reference.

II. ADDING DIPOLE FIELD HARMONICS

To improve RHIC's model-to-machine agreement, as well as use all relevant knowledge accumulated during the collider's construction and commissioning [11, 12], the RHIC online model was built such that it would include the sextupole field harmonics b_2 of all sector bends (sbends) and the corresponding feed-down effects on the betatron tunes. These harmonics are found in `magbase`, one of RHIC's three major databases [13], along with all normal and skew components $a_n, b_n, n = 1, \ldots, 10$ (where $n = 1$ is the quadrupole order, etc) as measured during both cold and warm testing at different current excitations in 1994-97. Only a limited number of sbends were measured cold: their data is stored in the `Magz` table. Other sbends with only warm measurements have their field harmonics split between two tables depending on which region was being measured:

- the *Lead* and *Return* ends of the sbend can be found in the `EndsHarm` table;
- the measurements integrated over the length of the magnet are in `BodyHarm`.

From either of the tables mentioned above, the $b_2\,[j]$ value at a given current I for the jth sbend of a given list can be converted into an integrated sextupole gradient $K_2L\,[j]$ via:

$$K_2L\,[j]\,(I) = \frac{\left(2.0 * b_2\,[j]\,(I) * 10^{-4}\right) * L_j}{\rho_j * R_j^2} \tag{1}$$

where L_j is the mechanical length of that jth sbend, ρ_j its curvature and $R_j = 25$ mm the reference radius for that measurement. The 10^{-4} coefficient is applied as a renormalization from the $b_0\,[j]$ main field harmonic typically given as 10^4 for this type of measurement. Instantiated polynomial functions $K_2L\,[j]\,(I)$ exist for every sbend installed in the RHIC ring (and a handful of spares), and are generated in only a few steps.

A. Fitting constraints

Given that the operating currents for sbends in RHIC and HSR range from 400 Amps to nearly 6000 Amps, it is more appropriate to fit for polynomials in $(I - I_{\text{ref}})$ to prevent the larger currents to skew the function. I_{ref} is chosen as 3200 Amps.

B. Geometry of sbend edges

To first order, the sextupole harmonics at the *Lead* (b_2^B) and *Return* (b_2^A) edges are dominated by the geometrical shape of the sbend coil windings. As such, the corresponding integrated gradients $K_2^B L$ and $K_2^A L$ can be taken as constant through the range of operating currents of 400-600 Amps, and do not need to be fitted to any function.

C. Fitting the *Body* harmonics

For all sbends measured **cold**, their *Body* K_2L terms are derived from fitting Equation 1 as either a 10th-order polynomial (long sbends *DRG*) or a 9th-order one (shorter sbends *DRX* and *DRZ*, removed for the HSR).

For long sbends only measured **warm** or with too few cold measurements (typically less than 9 data points), each $K_2L\,[j]$ is reconstructed using an empirical warm-to-cold transfer function:

$$K_2L\,[j]\,(I, w\,[j]) = P\,(I - I_{\text{ref}}) + w\,[j] \cdot Q\,(I - I_{\text{ref}}) \tag{2}$$

where $w\,[j]$ is the warm $K_2L\,[j]$ calculated from a $b_2\,[j]$ measurement at $I = 30$ Amps. P and Q are aggregate polynomials derived from a linear regression between warm and cold measurements of the combined data of all sbends with enough "cold" data points. For each of these sbends, a linear warm-to-cold fit at each current along the "up" side of the cold measurement process gives current-dependent intercept and slope terms. The series of intercept terms is then fit to a 10th-order polynominal in $(I - I_{\text{ref}})$, while the series of slope terms is parameterized to 9th-order.

D. Specific case of shorter sbends

The HSR will inherit all RHIC sbends except the DRX and DRZ ones which were enabling various crossing trajectories for hadron bunches through the center of each insertion region when moving between inner and outer arcs. The remaining HSR sbends are sorted into three categories:

1. DRG and DR8: long arc sbends – 9.441 meters long;
2. D96: short dispersion suppression sbends – 2.949 meters long;
3. D5I and D5O: shorter, bridges the difference between inner/outer arcs – 6.916 and 8.698 meters long respectively.

One therefore needs to adjust the fitting from Equation 2 such that:

$$K_2L\,[j]\,(I, w\,[j]\,, f\,[j]) = f\,[j] \cdot P\,(I - I_{\text{ref}}) + w\,[j] \cdot Q\,(I - I_{\text{ref}}) \tag{3}$$

where $f\,[j]$ is the ratio of lengths L_j / L_{DRG}.

E. Implementation in models

With all *Body*, *Lead* and *Return* integrated gradients from sextupole harmonic having been instantiated via the process described above for every HSR sbend, the next step is to add them to the lattice model as an update to the `250730a` baseline release, available as both MAD-X/Xsuite and Bmad inputs.

While the methodology is different between the two codes, the concept is identical: rather than rewrite the definition of each sbend, it is possible to amend it with the *Body* gradient $K_2\,[j]$ (instead of the integrated value). There is however another important matter to take into account: how the sbends were installed in the RHIC tunnel, not just their orientation but their positioning with respect to the surrounding elements.

1. Orientation

The RHIC Configuration Manual [14] details the conventions used for the installation of all magnets, in particular for sbends:

> *"For RHIC, the convention defining the "installed" direction of the main dipole and quadrupole magnets in both rings refers to the Blue ring, in which the beam travels clockwise (CW). Extending this convention to corrector magnets has the ring-wide consequence that a clockwise installation in the Blue ring implies that the beam enters the non-Lead end, whereas in the Yellow ring clockwise installation implies beam entering the Lead end of any magnet. All arc dipoles are CW installed."*

For the counterclockwise version of `250730a` shown in Figures 1 and 2, this means that two new elements must be added around each sbend to represent the K_2L field at these edges. This can be done using thin-lens elements like e.g. `MULTIPOLE` in MAD-X/Xsuite, which takes an array $K_nL = \{K_0L, K_1L, K_2L \dots\}$ as input. According to the Configuration Manual, in the counterclockwise HSR direction the sequence of elements should therefore be: $Lead - Body - Return$.

2. Positioning during installation - Feed-down effects

During construction and assembly of RHIC [11, 12] all sbends were displaced radially outwards. In doing so, their magnetic center is not aligned with the expected trajectory of the hadron bunches traveling through: this small displacement $\Delta x = 1.27$ mm leads to a betatron tunes feed-down from the $K_2L\,[j]$ harmonic that can be represented by a quadrupole integrated gradient given by:

$$K_1L\,[j] = 2. \cdot K_2L\,[j] \cdot \Delta x \ . \tag{4}$$

This feed-down is only generated by the *Body* sextupole harmonic components, since it is reported that the sbend displacement was done such that the bunches are kept on-axis at the *Lead* and *Return* ends [11]. In later RHIC runs, the model value for Δx was adjusted empirically to 2.794 mm in order to provide the strongest model-to-machine agreement on measured betatron tunes and linear chromaticities.

The corresponding *Body* quadrupole gradient $K_1\,[j]$ are therefore added to the definition of sbends in the HSR lattice models, along with the sextupole gradient $K_2\,[j]$ as already mentioned earlier.

III. IMPACT OF THE CHANGES TO THE REFERENCE LATTICE

Atfer turning the lattice around and implementing the sextupole harmonics, a new Twiss table is calculated. Table II shows a comparison of the `250730a` baseline betatron tunes and chromaticity with and without the new harmonics. While the betatron tunes change by moderate amounts (-0.034 horizontally and +0.036 vertically), the chromaticities in both planes change by over 5 units (-5.44, +6.88 respectively).

TABLE II: Changes in the HSR `250730a` lattice for 275 GeV polarized protons with/without the sbends K_2 harmonics.

Parameter	Without K_2 harmonics	With K_2 harmonics
Transition gamma γ_t	22.58	22.55
Momentum compaction α_c	1.96×10^{-3}	1.97×10^{-3}
Working point Q_x, Q_y	28.228, 27.210	28.194, 27.246
Chromaticities χ_x, χ_y	2.00, 2.00	−3.44, 8.88

The HSR is designed to enforce synchronicity with the ESR at the IP6 collision point by adjusting its circumference via radially shifting the trajectory of hadron bunches in the arcs [15]. Since Table II shows the significant impact of the sextupole harmonics of sbends, it is paramount for chromaticities to be well under control in order to avoid even larger unwanted effects from operating the HSR with large orbit excursions in the arcs.

In addition to correcting the affected lattice parameters, one can also – with little added efforts – rein in the second- and third-order chromaticity terms $\chi^{(2)}, \chi^{(3)}$ derived from the betatron tunes variation with the relative momentum offset δ:

$$\Delta Q_{x,y}\,(\delta) = \chi_{x,y} \cdot \delta + \chi^{(2)}_{x,y} \cdot \delta^2 + \chi^{(3)}_{x,y} \cdot \delta^3 + \dots \ . \tag{5}$$

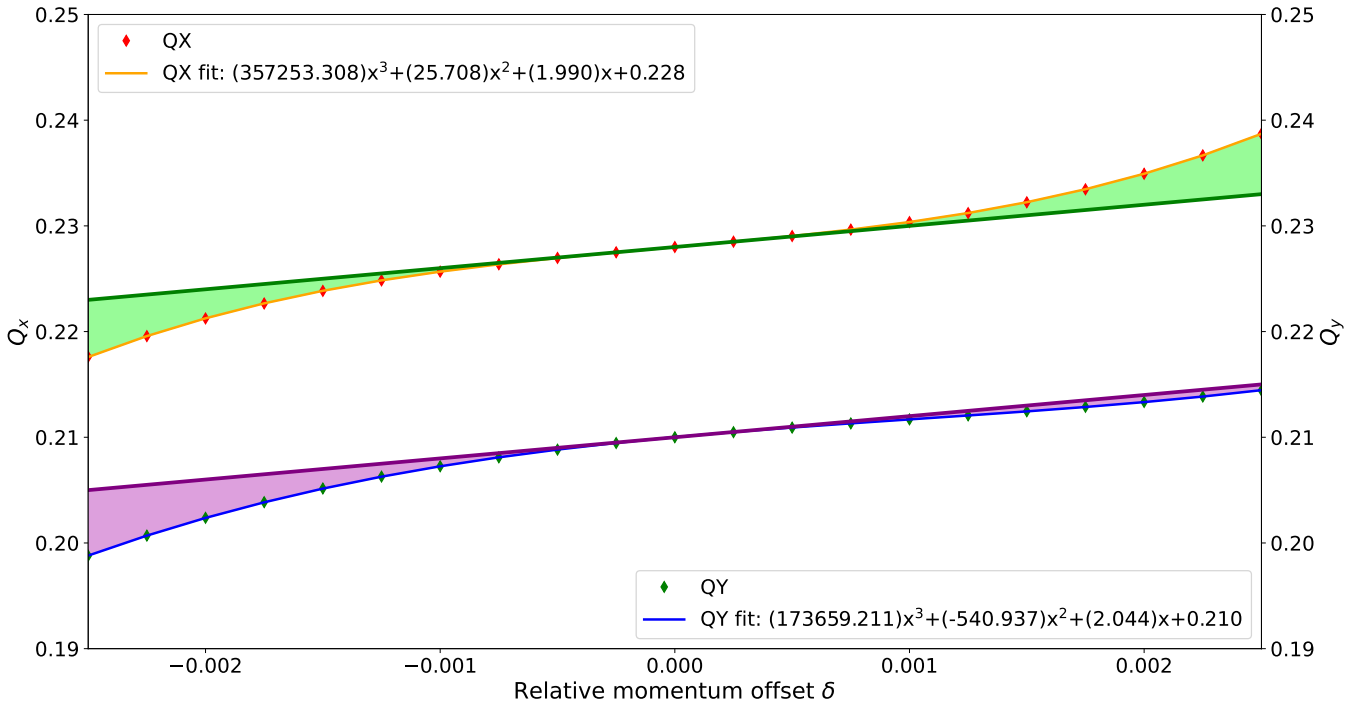

FIG. 3: Betatron tunes $Q_{x,y}$ as a function of momentum offset δ for the HSR 250730a baseline without sextupole harmonics. The result of a cubic fit of the tune curves giving the calculated values of $\chi^{(2)}_{x,y}$ and $\chi^{(3)}_{x,y}$ based on Equation 5 is included.

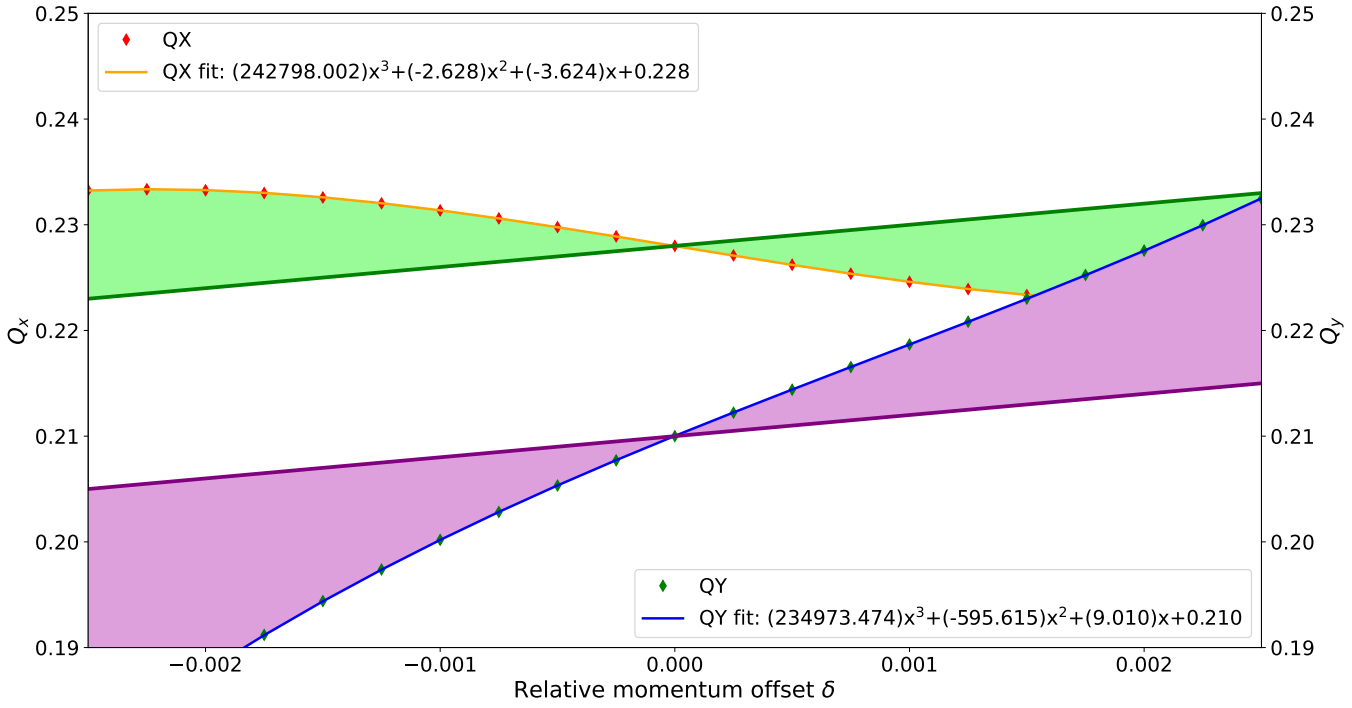

FIG. 4: Betatron tunes $Q_{x,y}$ as a function of momentum offset δ for the HSR 250730a baseline with sextupole harmonics and adjusted tunes. The result of a cubic fit of the tune curves giving the calculated values of $\chi^{(2)}_{x,y}$ and $\chi^{(3)}_{x,y}$ based on Equation 5 is included.

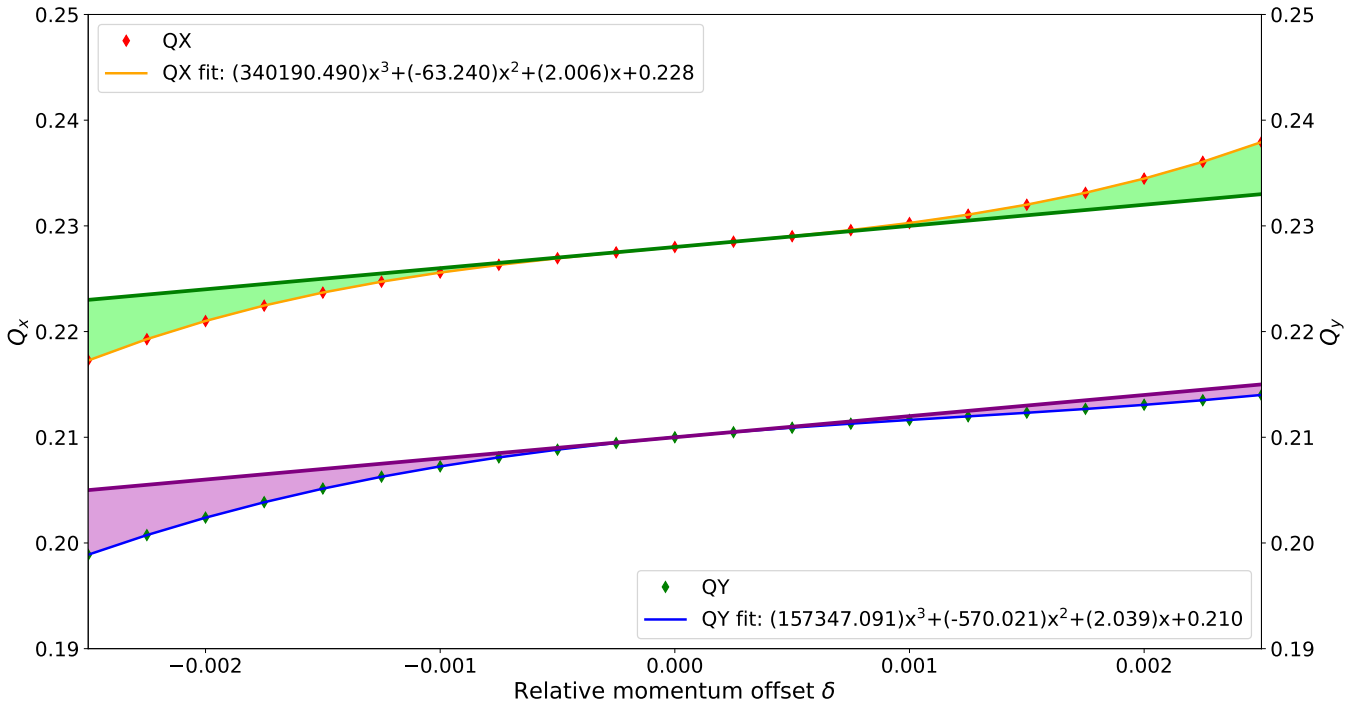

FIG. 5: Betatron tunes $Q_{x,y}$ as a function of momentum offset δ for the HSR 250730a baseline with sextupole harmonics and after correcting the linear chromaticity back to +2 units using 2 families of chromatic sextupoles. The result of a cubic fit of the tune curves giving the calculated values of $\chi^{(2)}_{x,y}$ and $\chi^{(3)}_{x,y}$ based on Equation 5 is included.

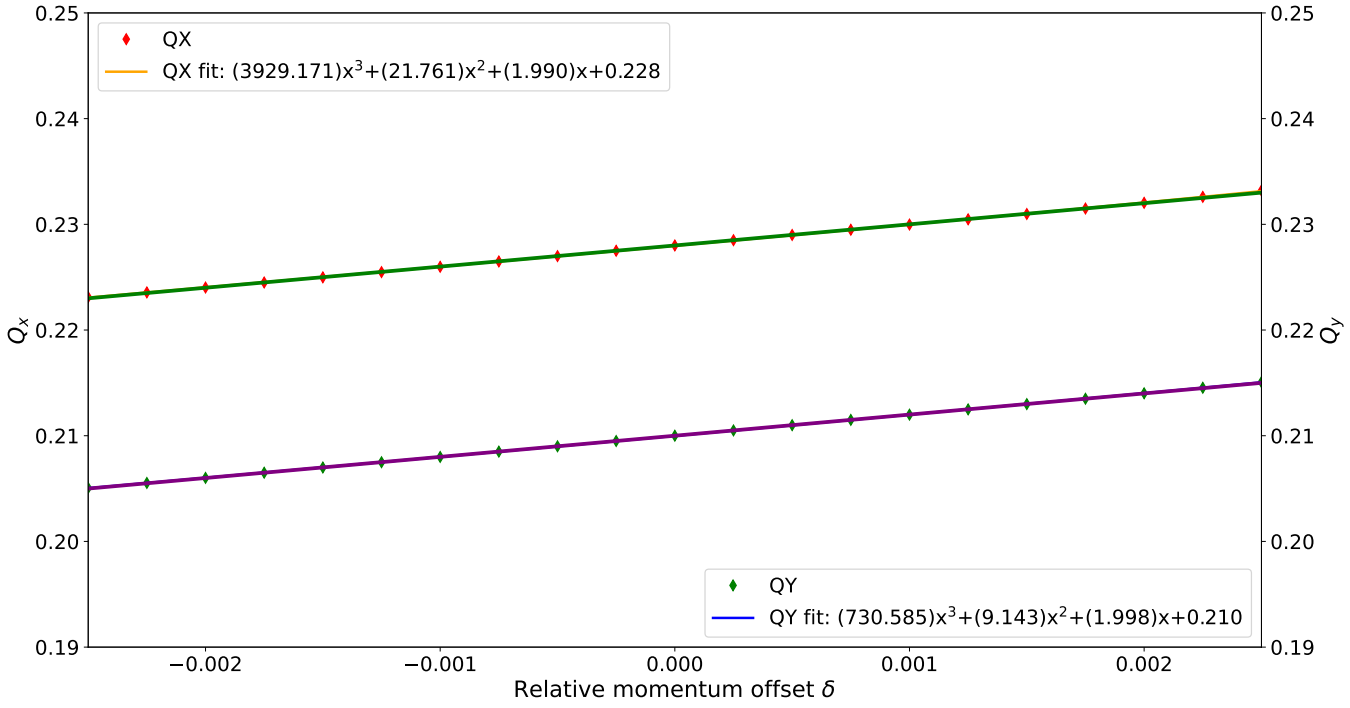

FIG. 6: Betatron tunes $Q_{x,y}$ as a function of momentum offset δ for the HSR 250730a baseline with sextupole harmonics and after minimzing the second- and third-order chromaticity terms using 24 families of chromatic sextupoles. The result of a cubic fit of the tune curves giving the calculated values of $\chi^{(2)}_{x,y}$ and $\chi^{(3)}_{x,y}$ based on Equation 5 is included.

The HSR has access to 24 families of chromatic sextupoles in the arcs i.e. two families per arc and per plane. Therefore the same methodology that was used in RHIC to correct non-linear chromaticity [16] can be applied to the HSR. Figures 3, 4, 5 and 6 highlight the impact of the K_2 harmonics and show the results of correcting the non-linear chromaticity terms $\chi^{(2)}_{x,y}$ and $\chi^{(3)}_{x,y}$ using the full set of 24 families: the linear chromaticity is rematched to its nominal target of +2 units for $\delta = 0.$ and kept practically linear over a range $\delta = \pm 2.5 \times 10^{-3}$.

IV. CONCLUSIONS

The baseline `250730a` HSR lattice has been flipped to properly account for the counterclockwise motion of hadron bunches in that ring, and the sign of all magnetic strengths up to sextupole order have been adjusted accordingly. The rigidity-dependant instantiated b_2 sextupole field harmonics of all arcs dipoles have been added to the HSR model based on available warm and cold measurement stored in the `magbase` database. The inclusion of the b_2 in the dipoles is consistent with the best modeling practices for RHIC operations. The corresponding feed-down effects due to the necessary misalignment of RHIC dipoles during construction was also added to the model.

Noticeable deviations in betatron tunes and linear chromaticities were observed then corrected, along with the first two orders of non-linear chromaticity terms using all 24 chromatic sextupole families available. This was an important step in upgrading the HSR model for further development of radially shifted lattices, made necessary to establish synchronicity at IP6 between HSR hadron bunches and ESR electron bunches. Building on the succesful implementation of the b_2 sextupole fields, additional dipole field harmonics are being implemented in future iterations of the HSR lattice model in the context of evaluating the design of the new IR6 magnets, both warm and superconducting.

[1] S. Nagaitsev, in *Proc. IPAC'25*, International Particle Accelerator Conference No. 16 (JACoW Publishing, Geneva, Switzerland, 2025) pp. 878–882.

[2] J. Berg *et al.*, in *Proc. IPAC'23*, International Particle Accelerator Conference No. 14 (JACoW Publishing, Geneva, Switzerland, 2023) pp. 903–905.

[3] R. D. Maria *et al.*, in *Proc. IPAC'23*, International Particle Accelerator Conference No. 14 (JACoW Publishing, Geneva, Switzerland, 2023) pp. 3340–3343.

[4] G. Iadarola *et al.*, in *Proc. HB'23*, ICFA Advanced Beam Dynamics Workshop on High-Intensity and High-Brightness Hadron Beams No. 68 (JACoW Publishing, Geneva, Switzerland, 2024) pp. 73–80.

[5] D. Sagan, Nuclear Instruments and Methods in Physics Research Section A **558**, 356 (2006).

[6] D. Marx *et al.*, in *Proc. IPAC'24*, International Particle Accelerator Conference No. 15 (JACoW Publishing, Geneva, Switzerland, 2024) pp. 234–237.

[7] S. Kumar, Nuclear Instruments and Methods in Physics Research Section A: Accelerators, Spectrometers, Detectors and Associated Equipment **1069**, 169922 (2024).

[8] W. F. Bergan, P. Baxevanis, M. Blaskiewicz, G. Stupakov, and E. Wang, in *Proc. IPAC'21* (JACoW Publishing, Geneva, Switzerland) pp. 1819–1822.

[9] H. Zhao, J. Kewisch, M. Blaskiewicz, and A. Fedotov, Physical Review Accelerators and Beams **24**, 10.1103/PhysRevAccelBeams.24.043501 (2021).

[10] W. Bergan *et al.*, in *Proc. IPAC'24*, International Particle Accelerator Conference No. 15 (JACoW Publishing, Geneva, Switzerland, 2024) pp. 234–237.

[11] S. Peggs, S. Tepikian, D. Trbojevic, and J. Wei, *The Warm Iron Geometry of the "Average" RHIC Dipole*, Technical Note RHIC/AP/62 (Brookhaven National Lab. (BNL), Upton, NY (United States), 1995).

[12] S. Peggs, *The Iron Geometry of RHIC Dipoles*, Technical Note RHIC/AP/94 (Brookhaven National Lab. (BNL), Upton, NY (United States), 1996).

[13] G. Robert-Demolaize, *The RHIC Database System*, Technical Note (Brookhaven National Laboratory, 2026) in preparation.

[14] Relativisitic Heavy Ion Collider Configuration Manual (Brookhaven National Laboratory, 2006), Final ed.

[15] G. Robert-Demolaize, A. Drees, H. Lovelace III, A. Marusic, F. Méot, S. Peggs, and M. Valette, Nuclear Instruments and Methods in Physics Research Section A: Accelerators, Spectrometers, Detectors and Associated Equipment **1070**, 170043 (2025).

[16] G. Robert-Demolaize, A. Drees, X. Gu, A. Marusic, S. Tepikian, M. Bai, and S. White, *Maximizing RHIC Deliverable Luminosity with Dynamic Telescopic Beta* Squeeze*, Tech. Rep. (Brookhaven National Laboratory (BNL), Upton, NY (United States), 2025).